

Multi-DFIG Aggregated Model Based SSR Analysis Considering Wind Spatial Distribution

Junjie Ma¹, Fang Liu^{1*}, Lin Jiang², Min Wu³, Yong Li⁴, Weiyu Wang⁴

¹ School of Information Science and Engineering, Central South University, Changsha 410083, China

² Department of Electrical Engineering and Electronics, University of Liverpool, Liverpool, UK

³ School of Automation, China University of Geosciences, Wuhan 430074, China

⁴ College of Electrical and Information Engineering, Hunan University, Changsha 410082, China

*csuliufang@csu.edu.cn

Abstract: This paper investigates the impact of wind spatial distribution on sub-synchronous resonance (SSR), considering wind speed difference and wind turbine division. For a doubly-fed induction generator (DFIG) wind farm, two equivalent aggregated models, i.e., a one-DFIG model and a multi-DFIG model, are established and both simplified to impedance model for investigation. In one-DFIG model, the SSR mechanism in DFIG wind farm, and the impact of wind speed on SSR are discussed. The concept of damping is introduced to explain how DFIG SSR current changes under the negative resistance of wind farm. Then, in multi-DFIG model, DFIGs are divided into different groups based on their wind speed, and the interaction between DFIG groups is investigated. Simulations are used to validate the proposed analysis, and the results show that, multi-DFIG model performs a higher accuracy when dealing with DFIG wind spatial distribution problems compared with one-DFIG model.

1. Introduction

With a low environment impact and technical development, wind power has been exploited worldwide. In countries with vast land area, large-scale wind farms are usually located far from load centres due to the distribution of wind resources [1]. The utilization of wind energy highly relies on high-rating and long-distance power transmission. Series capacitor compensation technology is proved to be an efficient and economical way to increase transfer capacities of existing long-distance AC transmission lines. However, sub-synchronous resonance (SSR), an oscillation at a frequency below power frequency, is introduced to generator when it exchanges significant energy with series capacitor compensated transmission system [2]-[4]. In recent years, many wind farm SSR accidents have been reported. For instance, in October 2009, America, the wind farms connected to the Electric Reliability Council of Texas (ERCOT) suffered a serious SSR accident due to the operation of the series capacitor groups [4], [5]. In December 2012, SSR was observed in wind farms located in the northern China. This SSR accident was also caused by series compensated capacitor groups, and occasionally happened in the next few weeks [6].

Doubly-fed induction generator (DFIG) is widely installed all over the world due to its high capability, low investment, and flexible control [7]. As DFIG is especially vulnerable to SSR instability, many researches on DFIG SSR have been carried out. DFIG wind farm to series compensated capacitor systems are usually simplified to impedance model for SSR analysis [8]-[10]. Impacts of wind speed, compensation level and control gains on SSR have been discussed in impedance models [11]-[13]. The spatial distribution of wind speed is proved to be one of the key parameters that impacts on wind farm SSR [14]. To reduce computational complexity, turbines in a wind farm are often aggregated when modeling [15], [16]. In previous works, a wind farm is usually presented by a one-machine

aggregated model with the assumption that all wind turbines are working under a same working condition. However, in a wind farm, wind turbines is spatially located, and wind speed is spatially distributed in a wide area [17]. The performance of the one-machine model is unsatisfactory when wind turbines have different parameters or work under different conditions [18]-[20]. Especially the coupling behaviors and the interactions between wind turbines are ignored in the one-machine model when analyzing the impact of wind speed on SSR.

The contribution of this paper is to analyze the impact of wind spatial distribution on SSR and provide an analytical method on the interactions between DFIGs when facing SSR incident. Wind speed distribution is considered as two aspects, respectively: 1) DFIGs may work under different wind speeds, and 2) when DFIGs with similar wind speed are aggregated to one group, turbine number of different aggregation groups may be different. Two aggregated DFIG models, one-DFIG model and multi-DFIG model, are established. In the one-DFIG model, the impact of wind speed on SSR is investigated, and the concept of damping is introduced to explain how DFIG SSR current changes under the DFIG negative resistance. In multi-DFIG model, the interaction between DFIGs with different parameter settings is discussed. In the simulation, two aggregated models are put into comparison to discuss the impact of wind spatial distribution on SSR.

The rest of the paper is organized as follows. The study systems of two aggregated models are given in section 2. In Section 3, mechanism of SSR is discussed based on the proposed impedance models. Simulation studies are presented in section 4, and the conclusions draw in section 5.

2. Study System

In the study system, a DFIG wind farm has an entire capacity of $2n$ MW from aggregation of n DFIGs with capacity of 2 MW. DFIGs are connected to an aggregation bus in parallel. The wind farm is connected to load through a

series compensated transmission line. The configuration of the power system is shown in Fig. 1. In Fig. 1 (a), the DFIG wind farm is represented by a one-DFIG aggregated model. In Fig. 1 (b), DFIGs are divided into N DFIG groups, orderly, G-1, G-2, ..., G- N , and each group is represented by a one-DFIG aggregated model. The DFIG wind farm is equal to an N -DFIG aggregated model. The division of DFIG group is based on the value of wind speed. Specifically, when $N=2$, the wind farm is equal to a two-DFIG aggregated model.

In Fig. 1, R_L and L_L are the resistance and the inductance of the load, respectively; R_l and L_l are the resistance and the inductance of the transmission line, respectively; R_W , L_W are the equivalent resistance and inductance of the DFIG wind farm, respectively. C_S is the value of the fixed series compensated capacitor. The compensation level k (from 0% to 100%) is

$$k = C_S/C \quad (1)$$

where C is the value of series capacitor when system is 100% compensated.

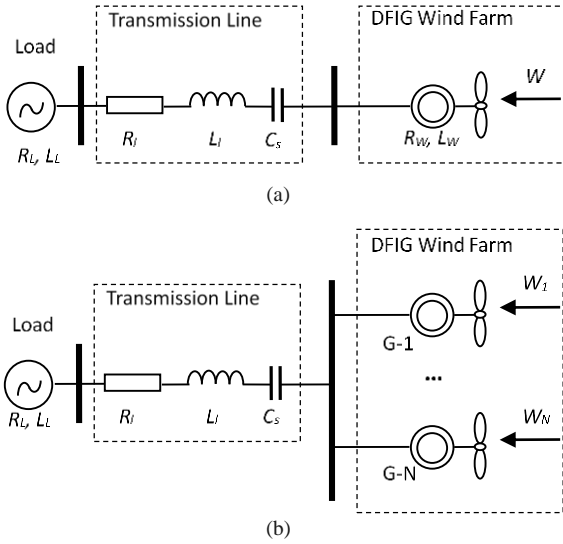


Fig. 1. Equivalent models of DFIG SSR study system when using *two different aggregated model*. (a) One-DFIG model; (b) Multi-DFIG model.

3. Impedance Model Analysis for DFIG Wind Farm

3.1. One-DFIG Aggregated Model

Assuming all DFIGs have same parameters and work at same work conditions, the wind farm can be simplified to a one-DFIG aggregated model. The impedance model of the study system in Fig. 1 (a) is shown in Fig. 2.

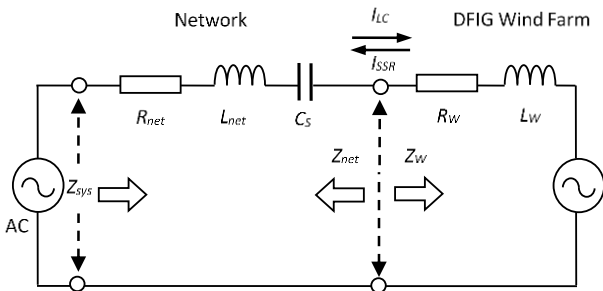


Fig. 2. Impedance of the one-DFIG aggregated model.

The impedance model consists two impedances:

respectively, the network impedance and the DFIG impedance. The impedance of the system Z_{sys} at frequency f can be written as

$$\begin{cases} Z_{sys}(f) = Z_{net}(f) + Z_W(f) \\ Z_{net}(f) = R_{net} + j\omega L_{net} + \frac{1}{j\omega C_S} \\ Z_W(f) = R_W + j\omega L_W \end{cases} \quad (2)$$

where R_{net} , L_{net} are the resistance and inductance of the network, respectively, and

$$\begin{cases} R_{net} = R_L + R_l \\ L_{net} = L_L + L_l \end{cases} \quad (3)$$

The series compensated capacitor and the inductance of the system forms a LC-loop and introduces LC oscillation current into the wind farm. The interaction between the LC current and the output current of the DFIG results an interference oscillation current I_f in the generator at SSR frequency. The relationship between power frequency f_0 , LC oscillation frequency f_{LC} , and SSR frequency f_{SSR} can be expressed as

$$\begin{cases} f_{SSR} = f_0 - f_{LC} \\ f_{LC} = \frac{1}{2\pi\sqrt{C_S(L_{net} + L_W)}} \end{cases} \quad (4)$$

When the impedance of the DFIG stator Z_{stator} , field branch Z_M , and rotor Z_{rotor} , are take into consideration, the impedance of the wind farm Z_W is comprehensively considered in [21] as

$$Z_W = \frac{Z_{DFIG}}{n} = \frac{Z_{stator} + Z_M \parallel Z_{rotor}}{n} \quad (5)$$

where Z_{DFIG} is the impedance of one DFIG, n is the turbine number. And we have

$$\begin{cases} Z_{stator}(s) = R_s + sL_s \\ Z_M(s) = sL_M \\ Z_{rotor}(s) = Slip(s)R'_r + sL_{lr} \end{cases} \quad (6)$$

where R_s and L_s are the resistance and the inductance of the stator, respectively; L_M is the excitation inductance; R'_s and L_s are the equivalent resistance and the inductance of the rotor, respectively; and $Slip$ is the slip of the induction generator.

When control gains of the rotor side converter (RSC) inner control loop K_{Pr}/K_{Ir} , and cross gain K_{Dr} are considered, R'_r can be written as

$$R'_r = R_r + K_{Pr} + \frac{s}{s - j\omega_0} K_{Ir} - jK_{Dr} \quad (7)$$

The S-domain format of the slip is

$$Slip(s) = \frac{s}{s - j\omega_r} \quad (8)$$

where ω_r is the rotating speed of the generator. ω_r can be denote as a function of wind speed W as

$$\omega_r = F(W) \quad (9)$$

For instance, a typical wind speed to generator rotating speed curve used in simulation is shown in Fig. 3.

We introduce SSR damping to describe the SSR in DFIG. The damping of the system on SSR D_{sys} is [20]

$$D_{sys} = \frac{R_{sys}}{2L_{sys}} \quad (10)$$

D_{sys} is consist of two parts, namely, the damping of the network D_{net} and the damping of DFIG wind farm D_W

$$D_{sys} = D_{net} + D_W = \frac{R_{net}}{2L_{sys}} + \frac{R_W}{2L_{sys}} \quad (11)$$

The output current of the DFIG I_W is

$$I_W = I_0 + I_{SSR} \quad (12)$$

where I_0 is the nominal output current of the wind farm, and I_{SSR} is the interface SSR current caused by the interaction between LC loop and the DFIG. I_0 is constant, and I_{SSR} is influenced by the SSR damping.

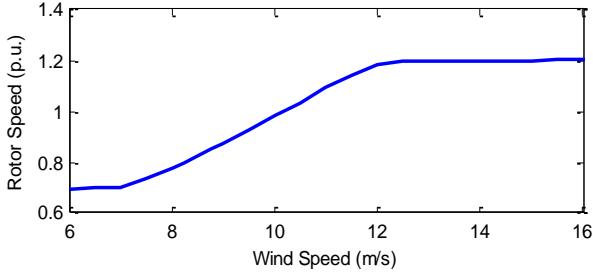


Fig. 3. Relationship between DFIG generator rotating speed and wind speed.

When LC current flows into the DFIG, the response process of DFIG can be considered as follows.

Firstly, we assuming that virtual current I_V is produce by DFIG as a reaction to the interference current I_f . With the SSR damping of the DFIG wind farm considered, I_V can be written as

$$I_V = I_f e^{-D_W f_{SSR} t} \quad (13)$$

Then, I_V is damped by the SSR damping provided by the network, and results in real SSR current I_{SSR} .

$$I_{SSR} = I_V e^{-D_{net} f_{SSR} t} \quad (14)$$

Combining (13) and (14), the relationship between I_{SSR} and D_{sys} can be given as

$$I_{SSR} = I_f e^{-(D_W + D_{net}) f_{SSR} t} \quad (15)$$

Finally, equation (15) shows how DFIG SSR current influenced by the damping ratio.

The slip of the induction generator is both influenced by wind speed and the compensation level. Obviously, when $f_{SSR} < f_r$, $Slip < 0$. The resistance of DFIG, as well as the SSR damping of the wind farm are negative. By (13), the wind farm can be considered as a SSR oscillation current source when $D_W < 0$. By (15), when $R_{net} + R_W < 0$, the SSR damping of the system $D_{sys} < 0$, the amplitude of the SSR current oscillatory grows. This is the induction generator effect (IGE) of DFIG.

The resistance of the DFIG is the determinable parameter on SSR. From analysis, the variation of wind speed will lead to the change of slip, as well as the change of the DFIG resistance. Other parameters that influence SSR are compensation level, control gains of RSC, and resistance of DFIG stator and rotor, respectively.

Meanwhile, when DFIGs have different resistances the equivalent resistance of the one-DFIG aggregated model can be present as

$$Z_W = Z_1 \parallel Z_2 \dots \parallel Z_n \quad (16)$$

where Z_1, Z_2, \dots, Z_n are the impedances of DFIG.

3.2. Multi-DFIG Aggregated Model

When wind turbines are spatial located in an area with non-uniform wind spatial distribution, DFIGs may work under different wind speeds and may have different resistances. To study the impact of wind spatial distribution on SSR, a multi-DFIG aggregated model presented in Fig.1 (b) will be used. The DFIGs under similar wind speeds are grouped, and a one-DFIG aggregated model represents each group. DFIG groups are integrated to the aggregation bus in parallel connection.

When the group number is chosen to be 2 ($N=2$), the multi-DFIG model is simplified to a two-DFIG model to release the complexity while is still eligible for wind spatial distribution analysis and DFIG interaction analysis. The wind farm consists two DFIG groups, G-1 and G-2, respectively. The impedance model of the two-DFIG model is shown in Fig. 4.

The impedance model is consists 3 impedances: respectively, the network impedance, the impedance of DFIG group G-1, and the impedance of DFIG group G-2. Denote the turbine number of G-1 and G-2 are l and m , respectively, the impedances of G-1 and G-2 are

$$\begin{cases} Z_1 = R_1 + j\omega L_1 = Z_{DFIG}/l \\ Z_2 = R_2 + j\omega L_2 = Z_{DFIG}/m \end{cases} \quad (17)$$

where R_1 and L_1 are the resistance and inductance of G-1 respectively; R_2 and L_2 are the resistance and inductance of G-2 respectively.

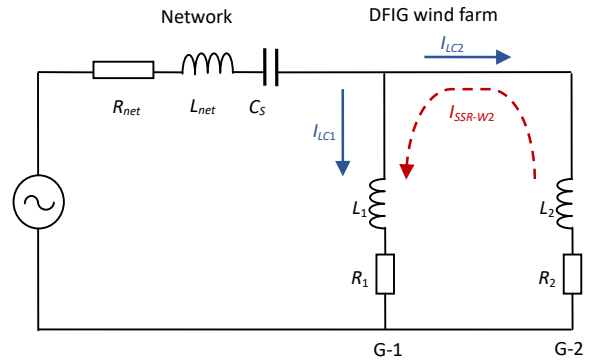


Fig. 4. Impedance of the two-DFIG aggregated model.

Assuming that G-1 works under a high wind speed and its resistance is positive ($R_1 > 0$), and G-2 works under a low wind speed and its resistance is negative ($R_2 < 0$), the damping contribution of G-1 and G-2 on SSR can be expressed as

$$\begin{cases} D_1 = \frac{R_1}{2L_{sys}} > 0 \\ D_2 = \frac{R_2}{2L_{sys}} < 0 \end{cases} \quad (18)$$

The interaction between G-1 and G-2 is described as follows:

Firstly, denote the interference oscillation current caused by LC current in G-1 and G-2 are respectively I_{f1} and I_{f2} , the virtual current output by G-1 and G-2 are

$$\begin{cases} I_{V1} = I_{f1} e^{-D_1 f_{SSR} t} \\ I_{V2} = I_{f2} e^{-D_2 f_{SSR} t} \end{cases} \quad (19)$$

Then, as the red dot line in Fig. 4 shows, the interference currents in G-1 and G-2 can be updated as

$$\begin{cases} I'_{f1} = I_{f1} + I_{V2} \\ I'_{f2} = I_{f2} + I_{V1} \end{cases} \quad (20)$$

where I'_{f1} and I'_{f2} are the updated interference current.

The updated interference current in DFIG is consist of two parts, respectively, the interference current caused by the LC oscillation, and the interference current provided by the nearby DFIG group. Therefore, the updated virtual current in G-1, I'_{V1} , is

$$I'_{V1} = I_{f1} e^{-D_1 f_{SSR} t} + I_{f2} e^{-(D_1 + D_2) f_{SSR} t} \quad (21)$$

And the updated virtual current in G-2, I'_{V2} , is

$$I'_{V2} = I_{f2} e^{-D_2 f_{SSR} t} + I_{f1} e^{-(D_1 + D_2) f_{SSR} t} \quad (22)$$

When $D_1 + D_2 < 0$, (21) is equal to

$$I'_{V1} = 0 + I_{f2}e^{-(D_1+D_2)fsst} \quad (23)$$

And when $D_1 + D_2 > 0$, (22) is equal to

$$I'_{V2} = I_{f2}e^{-D_2fsst} \quad (24)$$

From (24), it can be found that, due to its negative SSR damping, G-2 can be considered as a SSR current source that injects SSR current to nearby DFIGs. The SSR in G-2 is free oscillation when there is no external damping.

The format of (23) is consistent with the forced oscillation. That is to say, G-1 is forced to oscillate at SSR frequency by the oscillation source of G-2.

At the aggregation bus of DFIG wind farm, the virtual current of DFIG is

$$I_V = I'_{V1} + I'_{V2} \quad (25)$$

Finally, I_V is damped by the network, and results in real SSR current, which similar to (14)

The output current of two-DFIG aggregated model at the aggregation bus is

$$I_W = I_1 + I_2 + I_{SSR} \quad (26)$$

The equivalent impedance of the two-DFIG aggregated model is

$$Z_W = U_W/I_W \quad (27)$$

where U_W is the voltage of the aggregation bus.

4. Simulation Analysis

The cases are performed in SIMULINK. The wind speed and turbine numbers are adjustable, while other parameters are fixed. The system parameters are given in APPENDIX.

4.1. Impact of Wind Speed on SSR (in One-DFIG Aggregated Model)

The one-DFIG model in Fig. 1 (a) is used to analyze the impact of the value of wind speed on SSR. The relationship between the wind speed and the equivalent resistance of DFIG wind farm is shown in Fig. 5.

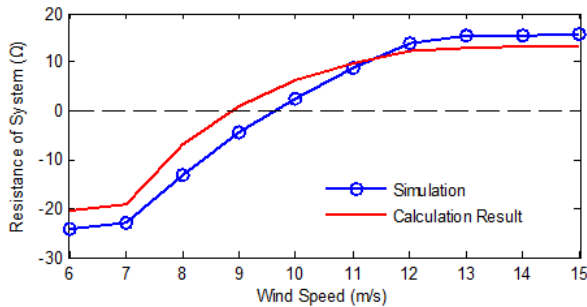


Fig. 5. Relationship between wind speed and equivalent resistance of the system.

In Fig.5, both calculation result by (5) and simulation show that, when wind speed increases, the resistance of the system increase. In simulation, when the wind speed is lower than 9.62 m/s, the resistance of the system is negative. In calculation result, when the wind speed is lower than 8.93 m/s, the resistance of the system is negative. The trend of the calculation result is consistent with the simulation. The average error between the calculation and the simulation result is 4.76 Ω. When all DFIGs are working under a same wind speed, the resistance calculation result by the one-DFIG impedance model is close to the simulation result.

Considering the dynamic wind speed variation, the DFIG SSR status when wind speed continuously variation is shown in Fig. 6. The initial wind speed of DFIG is 13 m/s,

and decreases from 13 m/s to 9 m/s during 0 second to 3 seconds. The SSR is observed from the electromagnetic torque of DFIG. It can be found that, when wind speed is 13 m/s, the SSR is hardly to be detected in DFIG. Along with the continuously decreasing of the wind speed, the SSR becomes more serious. The SSR is undamped during 2.5 seconds to 3 seconds while the corresponding wind speed decreases from 9.8 m/s.

Further, we select conditions of 3 sampling points as follows to intuitively observe the SSR status of DFIG:

Point A: $W = 7$ m/s. This sampling point represents the work condition of low wind speed;

Point B: $W = 10$ m/s. This sampling point represents the work condition of middle wind speed;

Point C: $W = 13$ m/s. This sampling point represents the work condition of high wind speed.

The corresponding rotating speed of point A, B and C are 0.706 p.u., 0.978 p.u. and 1.200 p.u., respectively. The time-domain simulation of the 3 sampling points are shown in Fig. 7. When the series capacitor is put into operation at 0.2 seconds, the SSR of point A is quickly mitigated within 0.3 seconds. The SSR of point B is maintained, and the SSR of point C rapidly diverges. By using mode analysis method, it can be found that the SSR frequencies of the 3 sampling points are both 28.2 Hz. When compensation capacitor is fixed, SSR frequency is determined by the inductance of the system. The variation of wind speed does not change the inductance and is independent of SSR frequency.

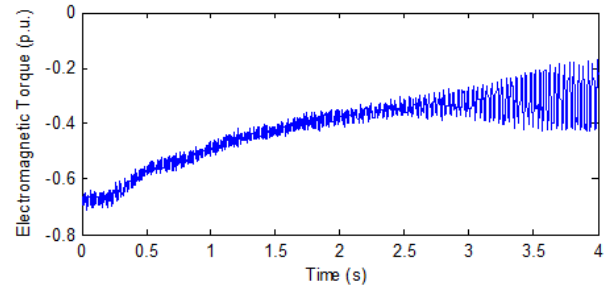


Fig. 6. The impact of wind speed variation on DFIG SSR.

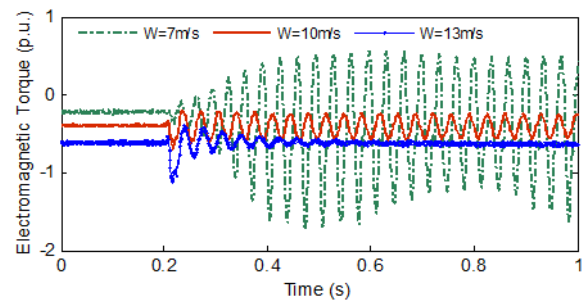


Fig. 7. SSR Status under different wind speeds.

4.2. Impact of Wind Spatial Distribution on SSR (in Two-DFIG Aggregated Model)

Following aspects are the consequences of wind spatial distribution: 1) Wind speed difference: DFIGs may work under different wind speeds; 2) Wind turbine division: DFIGs with similar wind speed should be divided into a same group, but the turbine number of different group may also different. For example, in a wind farm, there may 11 turbines work under 6 m/s, 9 turbines works under 7 m/s, 13 turbines works under 8 m/s, and 7 turbines works under 10 m/s [21]. Following cases are simulated in a two-DFIG

model to analyse the impact of wind speed spatial distribution on SSR.

Case 1: The turbine number in G-1 and G-2 are both 20. The wind speed of G-2 is fixed to 6 m/s.

Case 2: Wind speed for G-1 and G-2 are 13 m/s and 7 m/s, respectively. The turbine number in G-1 changes from 5 to 35, and the corresponding turbine number in G-2 changes from 35 to 5.

The relationship between wind speed difference and the system equivalent resistance under the condition of case 1 is shown in Fig. 8.

G-1 is given an initial wind speed of 6 m/s. When G-1 and G-2 are under low wind speed of 6 m/s, the equivalent resistance of the system is negative. The calculation result by (16) is -23.66Ω , and the simulation result is -17.42Ω . When the wind speed of G-1 increases from 6 m/s to 13 m/s, the resistance of the system increases from -23.66Ω to 2.32Ω in the calculation, and increases from -17.42Ω to 20.12Ω in simulation as a result of an increase of the equivalent resistance of G-1. The trend of the calculation result of the one-DFIG model and the simulation of the two-DFIG model are the same. However, when the wind speed difference becomes higher, the error of the calculation becomes larger. The average error between the simulation and the calculation result is 8.52Ω when the wind speed difference between G-1 and G-2 is lower than 2 m/s. However, when the wind speed difference is higher than 4 m/s, the average error is increased to 19.63Ω . The one-DFIG model may have a large error when dealing with the aggregation of DFIGs under high wind speed different.

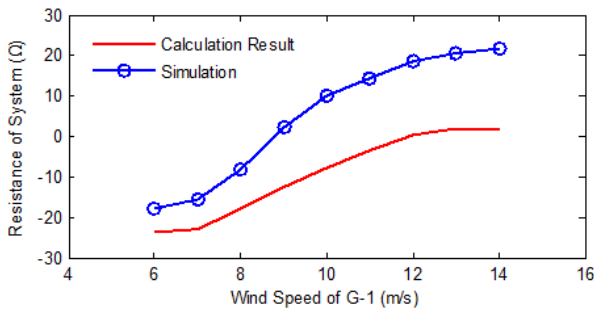


Fig. 8. Relationship between wind speed difference and equivalent resistance of the system.

The relationship between the wind turbine division and the equivalent system resistance under the condition of Case 2 is shown in Fig. 9. Meanwhile, to intuitively observe the SSR status, three DFIG divisions as follows are selected. Moreover, the simulation of these three divisions is shown in Fig. 10.

Division A: G-1 have 35 DFIGs, while G-2 have 5 DFIGs;

Division B: G-1 have 20 DFIGs, while G-2 have 20 DFIGs;

Division C: G-1 have 5 DFIGs, while G-2 have 35 DFIGs.

In Fig. 9, it can be found that when the turbine number of G-2 changes from 5 to 35, the resistance of the system increasing from 3.31Ω to 28.74Ω in the simulation of the two-DFIG model. However, the resistance of the system decreases from 10.53Ω to -17.84Ω in the calculation result of the one-DFIG model. The trend of the one-DFIG model and two-DFIG model are opposite to each other.

Time-domain simulation of Fig. 10 proves that DFIG division A has the worst SSR damping. SSR under the

condition of division A is approximately maintained, which means the equivalent resistance of the system is close to zero. On the contrary, SSR under the condition of division C is quickly mitigated within 0.4 seconds. The SSR trend of time domain simulation is inconsistent with the calculation result. The resistance of two DFIG groups is the real part in (17). The increase of turbine number results in a decrease of the absolute value of the DFIG group resistance. Therefore, under the condition of division A, the absolute value of resistance of G-1 is lower than G-2 consists more DFIGs, and the damping provided for SSR mitigation is also low. On the contrary, G-1 under the condition of division C can provide higher SSR damping than division A and B, since it consists of fewer DFIGs. Therefore, when dealing with the impact of DFIG division on SSR, the multi-DFIG model should be used instead of the one-DFIG model.

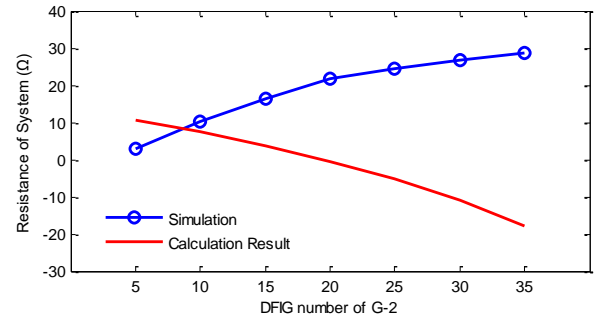


Fig. 9. Relationship between DFIG division and equivalent resistance of the system.

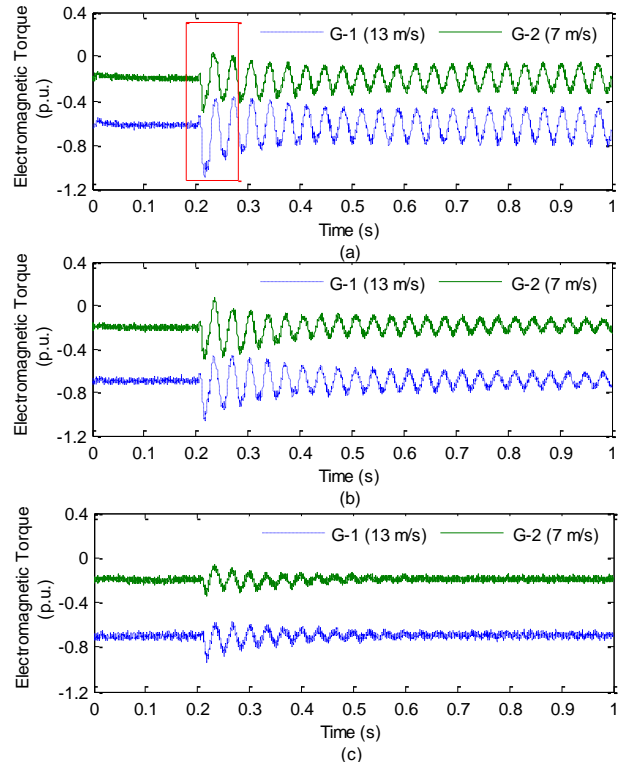


Fig. 10. SSR status of G-1 and G-2 under DFIG divisions. (a) Under Division A; (b) Under Division B; (c) Under Division C.

4.3. Interaction Between DFIG Groups

The detail of Fig. 10 (a) is shown in Fig. 11. The capacitor starts to oscillate at 0.2 seconds. At 0.232 seconds, G-2 meets its first SSR peak. 0.005 seconds later, G-1 meets

its first peak. Comparing the two SSR curves it can be found that G-2 always oscillates about 0.005 seconds faster than G-1. It can be inferred that the time difference Δt is the time that SSR current flows from G-2 to G-1. As the resistance of G-1 cannot provide enough damping to mitigate SSR of G-2, G-1 is forced to oscillate by the SSR current of G-2.

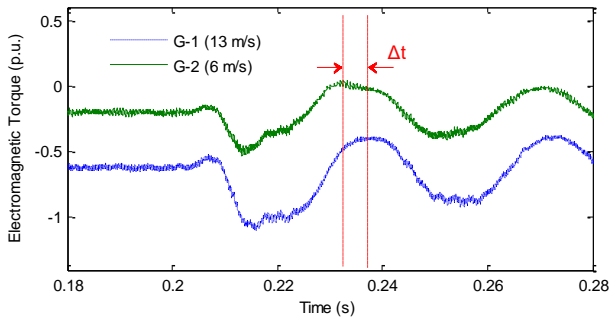


Fig. 11. Details of SSR status under DFIG division A.

The identified SSR mode of G-1 and G-2 in Case 2 are shown in Table 1. The signal is denoised by empirical mode decomposition, and then identified by Prony analysis. In Table 1, the SSR frequencies of G-1 and G-2 are almost the same. That is to say, the SSR modes of G-1 and G-2 are strongly coupled with each other. All DFIGs tend to oscillate coherently with similar oscillation frequencies. The result also proves that, when the total turbine number is fixed, the SSR frequency independent from the division of DFIGs.

Table 1 SSR mode of G-1 and G-2 in Case 2.

| Turbine number G-1 / G-2 | SSR Frequency of G-1 (Hz) | SSR Frequency of G-2 (Hz) |
|-----------------------------|------------------------------|------------------------------|
| 5 / 35 | 28.18 | 28.18 |
| 10 / 30 | 28.18 | 28.19 |
| 15 / 25 | 28.19 | 28.19 |
| 20 / 20 | 28.19 | 28.19 |
| 25 / 15 | 28.19 | 28.19 |
| 30 / 10 | 28.19 | 28.19 |
| 35 / 5 | 28.20 | 28.20 |

5. Conclusions

This paper has investigated the impact of the wind spatial distribution on SSR via proposing aggregated equivalent models for DFIG wind farms. The impact of wind speed on SSR is discussed based on the one-DFIG model where the interaction between DFIGs is discussed based on multi-DFIG model. The concept of damping is introduced to explain how the SSR current in DFIG changes under different situations. Following conclusions can be drawn:

1) DFIG under a lower wind speed has lower resistance and face more severe SSR problem. When the equivalent resistance of a DFIG is positive, it provides positive damping for SSR. On the other hand, DFIG with negative resistance reduces the damping for SSR and injects SSR current to nearby wind turbines. For this reason, a DFIG with negative resistance can be regarded as a SSR current source.

2) The calculation method of SSR damping of both equivalent models are investigated. The SSR status of the wind farm depends on the SSR damping provided by DFIGs. When the damping of the overall system is positive, the SSR in DFIG wind farm is mitigated.

3) SSR modes of DFIGs under different wind speeds are strongly coupled with each other. DFIGs with different resistances tend to oscillate at the same SSR frequency when SSR occurs, but with different types of oscillation. SSR in DFIG with negative SSR damping is free oscillation without external damping, while DFIG with positive damping may be forced to oscillate by nearby DFIGs with negative damping.

4) The multi-DFIG model is more accurate for wind farm SSR analysis than the one-DFIG model for dealing with a large wind speed differences and more suitable for considering the wind spatial distribution.

Future work could be done in analysing model performance of multi-machine model in actual wind farm.

6. Acknowledgments

This work was supported in part by the National Natural Science Foundation of China (NSFC) under Grant 61673398; by the 111 project under Grant B17040; by the Natural Science Foundation of Hunan Province under Grant 2018JJ2529; by the Huxiang Youth Talent Program of Hunan Province under Grant 2017RS3006.

7. References

- [1] Shi, R., Fan X., He Y.: 'Comprehensive evaluation index system for wind power utilization levels in wind farms in China', *Renewable and Sustainable Energy Reviews*, 2017, 69, pp. 461-471
- [2] IEEE SSR Working Group: 'Reader's guide to subsynchronous resonance', *IEEE Trans. Power System*, 1992, 7, (1), pp. 150-157
- [3] Anderson, P. M., Agrawal, B. L., Van Ness, J. E.: 'Subsynchronous resonance in power systems'. (John Wiley & Sons Press, 1999)
- [4] Leon, A. E., Solsona, J. A.: 'Sub-synchronous interaction damping control for DFIG wind turbines', *IEEE Trans. Power Systems*, 2014, 30 (1), pp. 419-428
- [5] Adams, J., Carter, C., Huang, S. H.: 'ERCOT experience with sub-synchronous control interaction and proposed remediation', *Proc. Transmission and Distribution Conference and Exposition (T&D)*, 2012 IEEE PES, Orlando, USA, May 2012, pp. 1-5
- [6] Wang, L., Xie, X., Jiang, Q., et al.: 'Investigation of SSR in practical DFIG-based wind farms connected to a series-compensated power system', *IEEE Trans. Power System*, 2015, 30 (5), pp. 2772-2779
- [7] Maghsoud, M., Khazaei, J., Nazarpour, D.: 'Sub-synchronous resonance damping via doubly fed induction generator', *Int. J. Electrical Power & Energy Systems*, 2013, 53 (4), pp. 876-883
- [8] Piyasinghe, L., Miao, Z., Khazaei, J., Fan, L.: 'Impedance Model-Based SSR Analysis for TCSC Compensated Type-3 Wind Energy Delivery Systems', *IEEE Trans. on Sustainable Energy*, 2015, 6(1), pp.179-187.
- [9] Fan, L., Kavasseri, R., Miao, Z., Zhu, C.: 'Modeling of DFIG-based wind farms for SSR analysis', *IEEE Trans. on Power Delivery*, 2010, 25 (4), pp. 2073-2082.
- [10] Liu, H., Xie, X.: 'Impedance Network Modeling and Quantitative Stability Analysis of Sub-/Super-Synchronous Oscillations for Large-Scale Wind Power Systems', *IEEE Access*, 2018, 6, pp. 34431-34438.
- [11] Zhu, C., Hu, M., Wu, Z.: 'Parameters impact on the performance of a double-fed induction generator-based wind

turbine for subsynchronous resonance control', IET Renewable Power Generation, 2012, 6 (2), pp. 92-98

[12] Miao, Z.: 'Impedance-model-based SSR analysis for type 3 wind generator and series-compensated network', IEEE Trans. Energy Conversion, 2012, 27 (4), pp. 984-991

[13] Vieto, I., Sun, J.: 'Small-signal impedance modelling of type-III wind turbine,' In Proc. General Meeting, IEEE PES, Denver, USA, July 2015, pp. 1-5.

[14] Zhu, C., Hu, M., Wu, Z.: 'Parameters impact on the performance of a double-fed induction generator-based wind turbine for subsynchronous resonance control', IET Renewable Power Generation, 2012, 6 (2), pp. 92-98

[15] Conroy, J., Watson, R.: 'Aggregate modelling of wind farms containing full-converter wind turbine generators with permanent magnet synchronous machines: transient stability studies', IET Renewable Power Generation, 2009, 3 (1), pp. 39-52.

[16] Luis, M. F., Francisco, J., José, R. S.: 'Aggregated dynamic model for wind farms with doubly fed induction generator wind turbines,' Renewable Energy, 2008, 33 (1), pp. 129-140.

[17] Towers, D. Paul, and L. J. Bryn: 'Wind turbine gust estimation using remote sensing data,' UKACC Int. Control Conf. pp. 349-354. Jul. 2014.

[18] Yang, F., Shi, L., Ni, Y.: 'Sub-synchronous oscillation analysis of complicated power grid incorporating wind farms with different types', J. Eng., 2017, 2017(13), pp. 1777-1782.

[19] Ma, J., Jiang, L., Wu, M., et al.: 'SSR analysis of DFIG based wind farm considering spatial distribution of wind speed', In Proc. General Meeting, IEEE PES, Boston, USA, July 2016, pp. 1-5.

[20] Li, Y., Liu, H., Chen, X.: 'Impact of PMSG on SSR of DFIGs connected to series-compensated lines based on the impedance characteristics', J. Eng., 2017, 2017(13), pp. 2184-2187.

[21] Liu, H., Xie, X., Zhang, C., et al.: 'Quantitative SSR analysis of series-compensated DFIG-based wind farms using aggregated RLC circuit model,' IEEE Trans. Power Systems, 2017, 32 (1), pp. 474-483.

8. Appendices

Table 2 Simulation parameters of the load, the transmission line, and the DFIG.

| Parameter | Value | Parameter | Value |
|-------------|---------------------------|-----------|------------|
| R_L | 0.864 Ω | R_s | 0.023 p.u. |
| L_L | 0.0229 H | L_S | 0.18 p.u. |
| R_l | 0.136 Ω/km | R_r | 0.018 p.u. |
| L_l | 0.032 H/km | L_r | 0.16 p.u. |
| C | 2.0723×10^{-5} F | L_m | 3.2 p.u. |
| Line Length | 400 km | k | 30% |